Microchimica Acta
https://doi.org/10.1007/s00604-018-2694-9

ORIGINAL PAPER

Hyaluronic acid functionalized nanostructured sensing interface for voltammetric determination of microRNA in biological media with ultra-high sensitivity and ultra-low fouling

Wei Wang[1] · Silambarasan Jayachandran[1] · Mengru Li[1] · Shenghao Xu[1] · Xiliang Luo[1]

Received: 16 November 2017 / Accepted: 18 January 2018

Abstract
An electrochemical biosensor for the detection of microRNA was prepared via chemical grafting of a Methylene Blue labeled reporter (MB-Rep) duplex onto a nanostructured surface that was obtained by electrodeposition of cobalt oxide and poly(o-phenylenediamine). This is followed by the attachment of hyaluronic acid and gold nanoclusters. In the presence of the target (microRNA), the probe-target duplex and the MB-Rep hairpin are formed. These will displace the labeled reporter from the sensor surface, and this results in a decrease of the amperometric signal for MB at a typical working voltage of −0.28 V (vs. Ag/AgCl). The electrode modified with hyaluronic acid possesses a large electroactive surface area and an excellent antifouling property. This makes it useful for ultrasensitive quantitation of microRNA even in complex biological media. The sensor has a linear response in the 100 f. to 0.1 μM microRNA concentration range, and a 33.3 f. detection limit. It was successfully applied to the determination of microRNA in cancer cells.

Keywords Electrochemical biosensor · MicroRNA · Hyaluronic acid · Nanostructure · Electrodeposition · Antifouling

Introduction

Tailored therapy develops rapidly with the abridged, label-free devices as fast and reliable tools for medical treatment. Thus, it is required to detect the biomarkers in human biological samples. However, the amount of biomarkers is usually very low, making it difficult to detect using the traditional methods [1]. Signal amplifying methods based on enzyme reactions have been developed, such as loop-mediated isothermal amplification [2], exponential amplification reaction [3, 4], rolling circle amplification (RCA) [5] and strand displacement amplification (SDA) [6]. Among these, SDA is the process through which two strands with partial or full complementarity hybridization to each other, displacing one or more pre-hybridized strands in the process. Strand displacement can be initiated at complementary single-stranded domains (referred to as toeholds) and progresses, through a branch migration process that resembles a random walk. By varying the strengths (length and sequence composition) of toeholds, the rate of strand-displacement reactions can be quantitatively controlled by a factor of 10^6 or so [7].

MicroRNAs are short (~22 nucleotides) noncoding RNA molecules. They have attracted increasing attention due to their vital feature as cancer biomarkers in cancer induction and evolution. Previous studies have found that the unusual behavior of microRNAs is related to the cell development, stress adaptation, and participates in a lot of forms of human cancers [8, 9]. The microRNAs are demanding not only in the control of cancers, but also in many other diseases such as cardiovascular diseases [10], neurological diseases [11] and immunological diseases [12]. Therefore, developing a fast, reliable and inexpensive method to monitor changes in microRNA biomarkers is of great importance.

Wei Wang and Silambarasan Jayachandran contributed equally to this work.

Electronic supplementary material The online version of this article (https://doi.org/10.1007/s00604-018-2694-9) contains supplementary material, which is available to authorized users.

✉ Xiliang Luo
xiliangluo@qust.edu.cn

[1] Key Laboratory of Sensor Analysis of Tumor Marker, Ministry of Education, College of Chemistry and Molecular Engineering, Qingdao University of Science and Technology, Qingdao 266042, China

Published online: 05 February 2018

For the recognition of microRNA, conventional analytical methods, including northern blot, reverse transcriptase-polymerase chain reaction (RT-PCR) and microarray based techniques, have been applied and shown some merits. But the limitations of the complicated operation, laborious and requiring expensive instrument restricted their further development. As consequence, biosensing strategies including electrochemical [13, 14], luminescence [15] and fluorescence biosensors [1, 16] have become a class of powerful tools for accurate and quantitative microRNA expression. Among these methods, electrochemical biosensors show great potential in serving as point-of-care diagnostics and multiplexed platforms for fast, simple and inexpensive nucleic acids analysis [17, 18].

The detection of microRNAs by electrochemical techniques has already achieved considerable attention. Even though, one critical issue for electrodes used in clinical samples is the nonspecific adsorption of materials such as proteins, lipids, cells and microorganisms, which lowers down the sensitivity of the electrodes and generates large noise signals, restricting the interactions between recognition elements and analytes, and limits the recognition of analytes at very low-concentration. Therefore, to lower down the nonspecific adsorption on the biosensor interface, the design and development of materials that hinder fouling are necessary to improve the accuracy and sensitivity of electrodes. Currently, one of the most efficacious ways to prevent the nonspecific binding of proteins is to make surfaces hydrophilic enough to retain a thin water layer on surfaces. In the past, zwitterionic polymers, synthetic peptides, PEG-based polymers and short chain molecules have been reported as low fouling materials with excellent antifouling ability [19, 20]. Remarkably, hyaluronic acid (HA) is anionic polysaccharide, incorporated with a repeated unit of disaccharide containing carboxyl (-COOH) groups, hydroxy (-OH) groups and amide groups (CO-NH) with superlative hydrophilicity which has been proved to be antifouling towards protein in previous studies [21, 22].

Here, we report on a novel antifouling electrochemical biosensor for the detection of microRNA-24 based on double-strand displacement reaction. The target binding with probe and replacing the redox labeled reporter (Methylene Blue, MB) leads to the decrease in signal of the biosensor. The antifouling property of the biosensor was demonstrated in the presence of human serum, and it displayed good analytical properties for microRNA-24 detection in biological complex media.

Materials and methods

Reagents

Cobalt nitrate hexahydrate, magnesium chloride, sodium chloride, sodium sulphate, o-phenylenediamine (OPD) and sulphuric acid were purchased from Aladdin Reagents (Shanghai, China,http://www.aladdin-e.com/). Methionine, $HAuCl_4 \cdot 3H_2O$, 11-mercaptoundecanoic acid (MUA), hyaluronic acid (HA) (MW 70 kDa) extracted from rooster comb, 1-ethyl-3-(3-(dimethylamino)propyl)-carbodiimide (EDC) hydrochloride and N-hydroxysulfosuccinimide (NHS) were purchased from Sigma-Aldrich Chemical Co (http://www.sigmaaldrich.com). Phosphate buffered saline (PBS, 0.2 M, pH 7.4, containing 0.9% NaCl) was used in all experiments. The human serum sample (serum was centrifuged for 10 min at 10,000 rpm, and then the collected supernatant was diluted by 0.2 M pH 7.4 PBS) was obtained from The Eighth People's Hospital of Qingdao, China. The MCF-7 cells were obtained from the tumor maker research center of the Cancer Hospital of Chinese Academy of Medical Sciences (Beijing China). All aqueous solutions were prepared using millipore water produced by a Milli-Q water purifying system.

DNA and RNA strands were supplied by Sangon Biotechnology Co., Ltd., (Shanghai, China, http://www.sangon.com/) and purified by high-performance liquid chromatography. Aminated probe, MB functionalized reporter and different targets of microRNA were used as received without further purification. The sequences of the various strands used in this work are shown in Table 1. All thermodynamic information was obtained using software available from The DINAMELT Web Server [23] managed by The RNA Institute at SUNY Albany. The Two state melting (hybridization) functions were used for double-strand binding calculations. Experimental parameters used for thermodynamic calculations were: 25 °C, 10 mM Na^+, 25 mM Mg^{2+} and 1.0 μM oligonucleotides.

Instruments and measurements

Electrochemical measurements were performed using a Gamry Reference 3000 Potentiostat (Gamry Instruments Co., USA,

Table 1 Oligonucleotide sequences and predicted thermodynamic complexation values

Materials	Sequence (5′ -3′)	MB-Reporter Gibbs energy (kcal/mol)	Probe Gibbs energy (kcal/mol)
Probe	NH_2–5'-CTG TTC CTG CTG AAC TGA GCC A-3'		
MB-Reporter	MB-5′-TGG CTC AGT TCA GCA GCC A-3'	−3.2	−22.3
miR-24	5'-UGG CUC AGU UCA GCA GGA ACA G-3'		−30.3
miR-141	5'-UAA CAC UGU CUG GUA AAG AUG G-3'		−3.0
miR-200	5'-CUG UGC GUG UGA CAG CGG CUG A-3'		−6.6
miR-429	5'-UAA UAC UGU CUG GUA AAA CCG U-3'		−2.8

https://cn.gamry.com/). A conventional three-electrode system was used, with an Ag/AgCl (3.0 M KCl) electrode as the reference electrode, a platinum wire as the auxiliary electrode, and modified glassy carbon electrode (GCE, 3.0 mm in diameter) as the working electrode. AC impedance spectra were recorded with DC bias potential of 0.25 V in a frequency range of 0.1 Hz to 100 kHz and AC amplitude of 0.005 V. Square wave voltammetry (SWV) experiments were used to detect target in PBS (0.2 M, pH 7.4) with the potential scanning range between −0.6 V and 0.0 V using pulse amplitude of 25 mV, pulse width of 20 ms, and an equilibrium time of 15 s. The peak current change at −0.28 V was measured and used as the biosensor response. Scanning electron microscope (SEM) was performed with a JEOL JSM-7500F SEM instrument (Hitachi High-Technology Co., Ltd., Japan, http://www.jeol.co.jp/en). Contact angle measurement was performed with a JC2000 Instrument (Shanghai Zhongchen instrument Co., China, http://www.shzhongchen.com/). High-resolution transmission electron microscopy (HRTEM) was performed on a JEOL JEM-2100 microscope operating at 200 kV. Dynamic light scattering (DLS) experiment was performed on a Zetasizer Nano-ZS (Malvern Instruments, Malvern, UK, http://malvern.cnpowder.com.cn). X-Ray photoelectron spectroscopy (XPS) analysis was performed using an AXIS Ultra spectrometer with a high-performance Al monochromatic source operated at 15 kV.

Synthesis of dual ligand functionalized au nanoclusters (AuNCs)

Dual ligand functionalized AuNCs were prepared according to our previous report [15]. Briefly, 350 μL of 1.0 M NaOH was added to 2.0 mL of 10 mM MUA solution. Then, 150 μL of 10 mM $HAuCl_4$ and 2.5 mL of 0.03 g mL^{-1} methionine were added to the above mixture. The mixture was left standing for 2 h at room temperature, and then the mixture was filtrated and the precipitate (AuNCs) was collected and dispersed in pure water.

Biosensor fabrication

The fabrication process of the antifouling biosensor was shown in Scheme 1. Initially, glassy carbon electrode (GCE) was polished with 0.3, 0.05 mm alumina slurries in sequence and ultrasonically washed with distilled water, ethanol, and ultrapure water for about 3 min, respectively. CoO was electrodeposited on the GCE surface in the solution containing 0.6 M $Co(NO_3)_2$ and 0.05 M $NaNO_3$ by applying a potential of −1.0 V for 100 s. Then, poly(o-phenylenediamine) (Popd) was polymerized on the CoO/GCE surface in two steps. Initially polymerization was carried out in 0.1 M Na_2SO_4 aqueous solution containing 10 mM opd then followed by 0.1 M H_2SO_4 aqueous solution containing 10 mM opd. Polymerization was performed with a potential cycle from −0.2 to 0.8 V vs. Ag/AgCl at a scan rate of 20 mV s^{-1} for 2 cycles. After electropolymerization, the Popd/CoO/GCE was rinsed several times with water. To covalently attach HA to the Popd (form bonds between free amine groups of Popd and carboxyl groups of HA), the modified electrode was immersed in 2.0 mg mL^{-1} HA, 50 mg mL^{-1} EDC and 50 mg/mL NHS at 37 °C for 120 min. Excess HA was removed by thorough washing with water, and then 50 mg/mL NHS and 50 mg mL^{-1} EDC was added to activate the carboxylic group

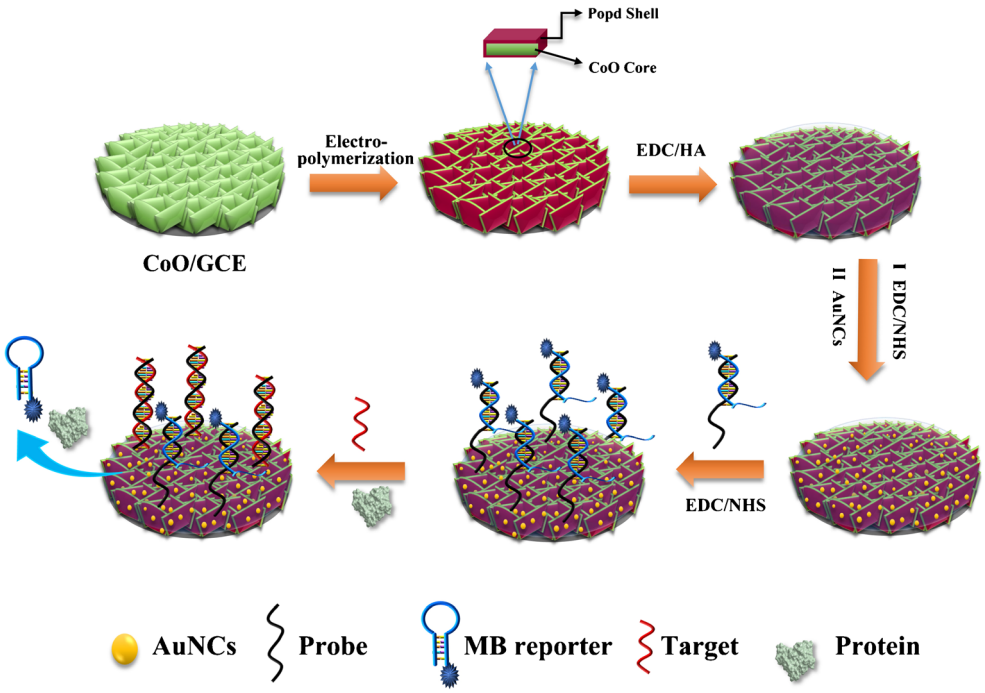

Scheme 1 Schematic illustration of the design and detection strategy

of HA in the HA/Popd/CoO/GCE, followed by the addition of 10 μM of methionine modified AuNCs. MB-rep/probe was prepared by adding 1 μL of MB-reporter to a solution containing 1 μL of probe at 60 °C for 2 h to form MB-rep/probe duplex. Finally, the immobilization of MB-rep/probe duplex on the modified electrode (Au/HA/Popd/CoO/GCE) was achieved through the formation of amide bonds between the amine groups of the probe (1.0 μM) and carboxyl groups of HA and AuNCs on the electrode surface, using EDC and NHS (50 mg mL^{-1}, respectively) as coupling reagents.

Gel electrophoresis analysis

The gel electrophoresis experiments were performed using a JY-SCZ2+ Electrophoresis Cell (Beijing Junyi-Dongfang Electrophoresis Equipment Co., LTD) equipped with a JY 300C Electrophoresis Power Supply (Beijing Junyi-Dongfang Electrophoresis Equipment Co., LTD, http://www.bjjunyi.com/). For the gel electrophoresis assay, samples (10 μL) were analyzed by 2% agarose gel in 50 x TAE (40 mM tris-acetic acid; 2.0 mM EDTA) at 160 V constant voltage for about 180 min at room

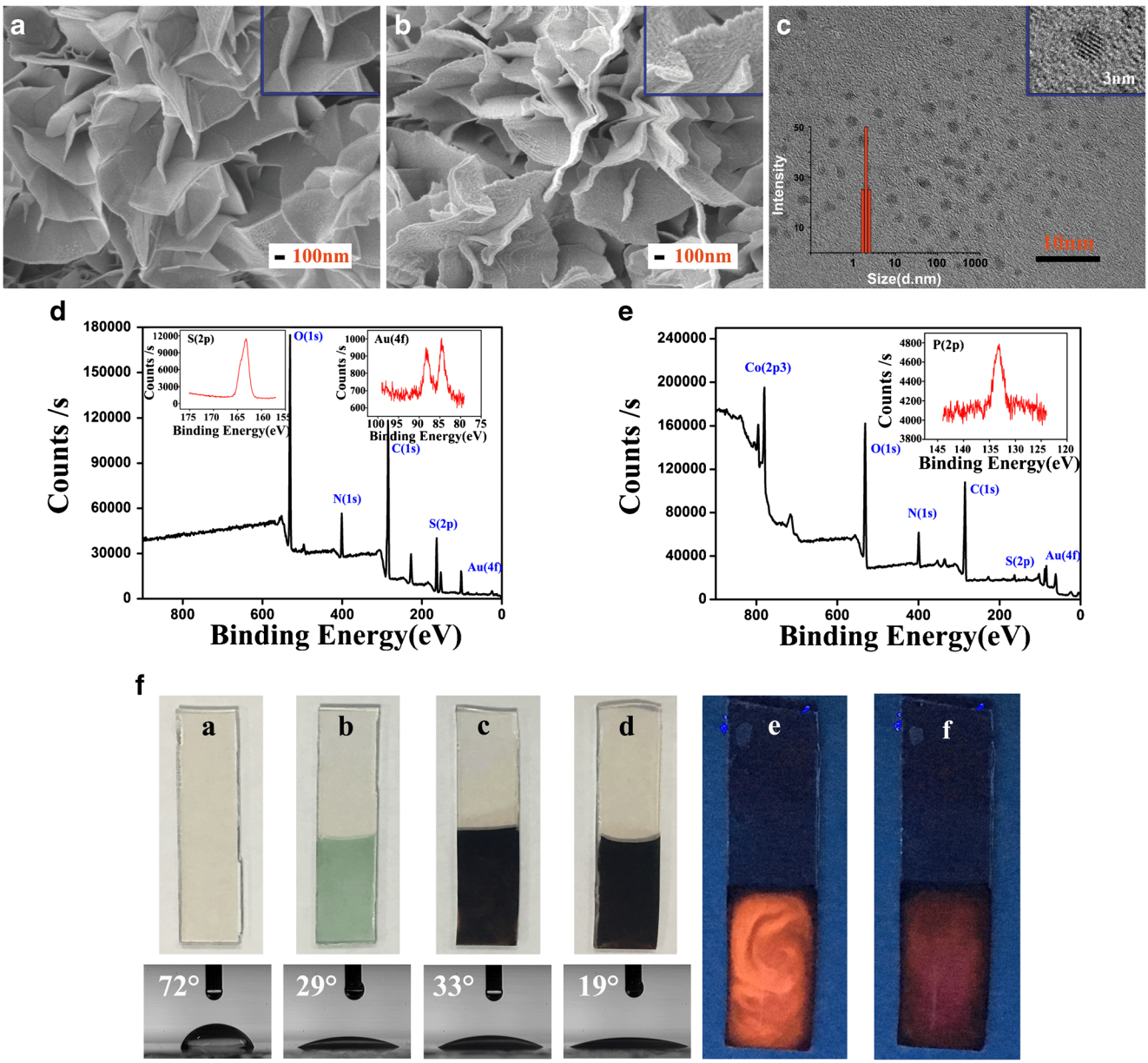

Fig. 1 SEM images of (**a**) CoO and (**b**) Popd/CoO core shell nanopetals; (**c**) TEM image of synthesized dual ligand AuNCs (inset, dynamic light scattering histogram of the Au NCs); XPS of (**d**) AuNCs and (**e**) MB-rep/probe/Au/HA/Popd/CoO/GCE; F) Photos and contact angle measurements of bare (**a**), CoO (**b**), Popd/CoO (**c**) and HA/Popd/CoO (**d**) modified ITO glass surfaces. (**c**) & (f) UV images of AuNCs and Au/HA/Popd/CoO modified ITO glasses

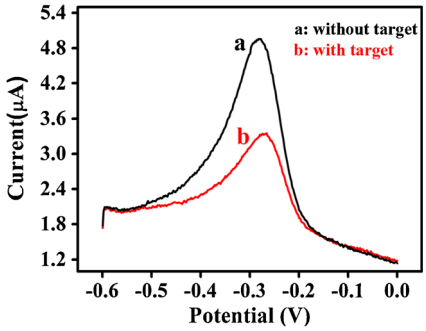

Fig. 2 SWV of the biosensor in PBS (0.2 M pH 7.4 PBS) without (black) and with (red) target microRNA

temperature. The gels were scanned using the Omega 16IC Gel imaging system (ULTRA-LUM, USA, http://www.scitech.com.au).

Results and discussion

Characterization of modified electrodes

In this work, CoO nanostructures with large surface area was deposited on the electrode, and OPD was then electropolymerized on the CoO surface to provide amine functional groups, for the further modification with HA, which can offer the electrode surface antifouling ability.

The morphology of the electrodeposited CoO nanostructure was first characterized with SEM. As shown in Fig. 1a, CoO displays the well-defined flowerlike nanostructure with the slender nanopetals growing vertically on the electrode surface. The thickness of the nanoflakes is around 40–50 nm. Morphology of the nanostructure was strongly dependent on the deposition potential by using electrodeposition method [24]. Previous studies have found that the CoO films prepared from $Co(NO_3)_2$ with electrodeposition exhibited a randomly porous structure with nanoflakes perpendicular to the substrate [25, 26], which are in consistent with our result.

The morphology of the poly(o-phenylenediamine) (Popd) coated CoO (Popd/CoO) is shown in Fig. 1b. Compared with the CoO nanopetals, the Popd/CoO nanopetals possesses larger thickness of about 60–70 nm, and the surfaces of these nanopetals are substantially coarsened with several wrinkles randomly distributed. This result clearly verified that Popd shell was formed on the surfaces of the CoO nanopetals. The thickness of the Popd shell can be well controlled by tuning the scan rate and the number of electrochemical deposition cycles. These Popd/CoO core/shell nanostructures provide high surface area and functional group for further modification.

XPS measurements were performed to characterize the elemental compositions of the synthesized AuNCs (with diameter of 2–3 nm, see Fig. 1c) and the biosensor interface. The detailed information about the peaks of all elements is provided in Table S1. The Au(4f) binding energies of AuNCs are at 88.38 and 84.51 eV respectively, which reveals that Au has two states [Au(0) & Au(I)) in the AuNCs [27] (Fig. 1d). The peak at 163.34 corresponds to S(2p) demonstrating the covalent interaction between AuNCs and sulfhydryl group [28]. Additionally, remaining peaks appeared on the XPS spectrum corresponds to C(1 s), N(1 s), O(1 s), and S(2p) reflecting that MUA and Methionine (dual ligand) stabilized AuNCs. The spectrum of Popd/CoO/GCE (Fig. S1 A) demonstrates the presence of Co(2p3), O(1 s), N(1 s) and C(1 s). After the modification with dual ligand AuNCs, the survey spectra of Au/HA/Popd/CoO/GCE (Fig. S1 B) clearly shows the presence of Au(4f) and S(2p). When the electrode is modified with MB-reporter/probe, a peak is observed at 133.3 eV corresponding to P(2p) which suggests that probe was covalently attached to the electrode surface (Fig. 1e and Fig. S1 C).

To characterize the wettability of the modified electrode surface, sessile drop method was used to determine the static water contact angles of bare, CoO, Popd/CoO and HA/Popd/CoO modified ITO glasses in air. Bare ITO glass has a contact angle of 72° (Fig. 1f), and the CoO modified ITO glass (green color) displays a lower contact angle of 29°, which might be ascribed to the hydroxyl groups of CoO. After the modification with Popd (brown color), the contact angle slightly increases to

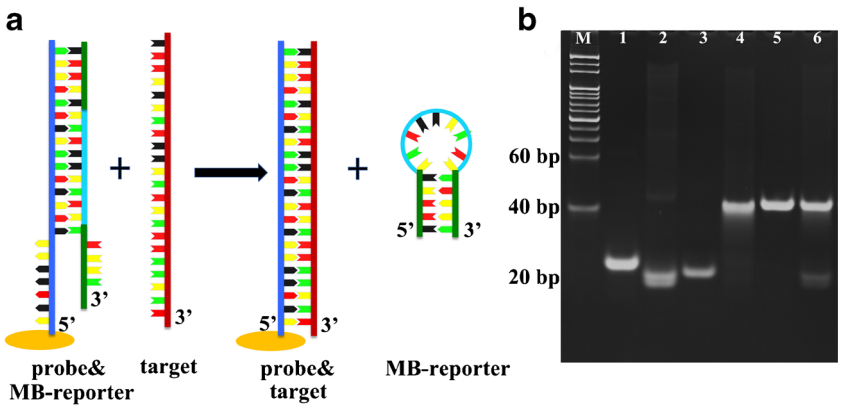

Fig. 3 **a** Detection mechanism of DNA displacement reaction, **b** Gel electrophoresis images of reaction products. Lane M, DNA marker (20–500 bp); lane 1–10 μM probe; lane 2–10 μM MB-rep; lane 3–10 μM target; lane 4–10 μM MB-rep/probe duplex; lane 5–10 μM probe with 10 μM target; lane 6–10 μM MB-rep/probe duplex with 10 μM Target

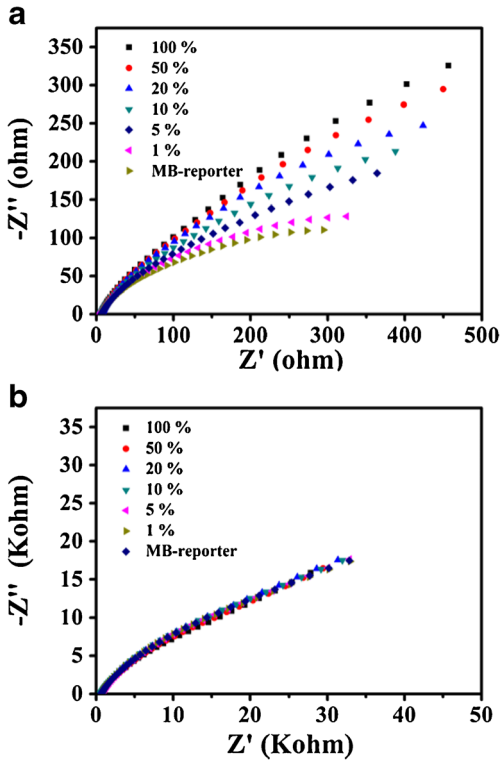

Fig. 4 EIS of the MB-rep/probe/Au/Popd/CoO/GCE (**a**) and MB-rep/probe/Au/HA/Popd/CoO/GCE (**b**) after soaking in various human serum samples

33°. The HA/Popd/CoO modified ITO glass presents a lower contact angle of 19°, displaying excellent hydrophilicity. The observed decreased contact angle suggests HA has better hydrophilicity, which is consistent with previous reports [29, 30]. Fig. 1f (e) and (f) present the UV images of AuNCs and Au/HA/Popd/CoO modified ITO glasses. AuNCs has fluorescence character [15] demonstrated by the luminous spot. However, when AuNCs are covalently attached to the HA/Popd/CoO surface, the luminous spot vanished, possibly owing to the fact that the energy of AuNCs is transferred to the underlying substrate.

Detection strategy and binding mechanism of microRNA

Owing to the presence of MB-reporter in the constructed biosensor, the square wave voltammetry (SWV) measurement of the biosensor showed a well defined peak at approximately −0.28 V (Fig. 2). After incubation in the solution containing target for 45 min, the peak current significantly decreased, which indicated that the MB-reporter was displaced by the target microRNA. Clearly, this current decrease associated with the target microRNA can be used for the assay of microRNA.

The design of the MB-reporter strand is very important as it can initiate strand displacement reactions, and then the partially double-stranded product will lead to further displacement reactions. The mechanism of the electrochemical detection of microRNA is schematically illustrated in Fig. 3a. Initially, partial double strands (probe/MB-reporter duplex) were formed on the electrode surface, as the sequence of MB-reporter was not exactly the same as the single strand of probe, and these partially double strands enabled further DNA displacement reactions. With the addition of target, the MB-reporter was displaced by the target rapidly, resulting in a complete double strand between the probe and the target. While the displaced MB-reporter was released tot he solution and folded into a hairpin structure. This displacement process was further verified by the theoretical calculation of the thermodynamic Gibbs binding energy (Table 1). The Gibbs energies of the probe-reporter, reporter hairpin and probe-target complexes are −22.3, −3.2 and −30.3 kcal mol^{-1}, respectively. All values were obtained using the Two State melting (hybridization) application available from the DINAMelt Web (http://unafold.rna.albany.edu/) Server at The RNA Institute at SUNY-Albany [23]. Formation of the complexes of probe-target (microRNA-24) is more favorable due to its more negative Gibbs binding energy compared with that of the hybridization to form probe-MB reporter complexes.

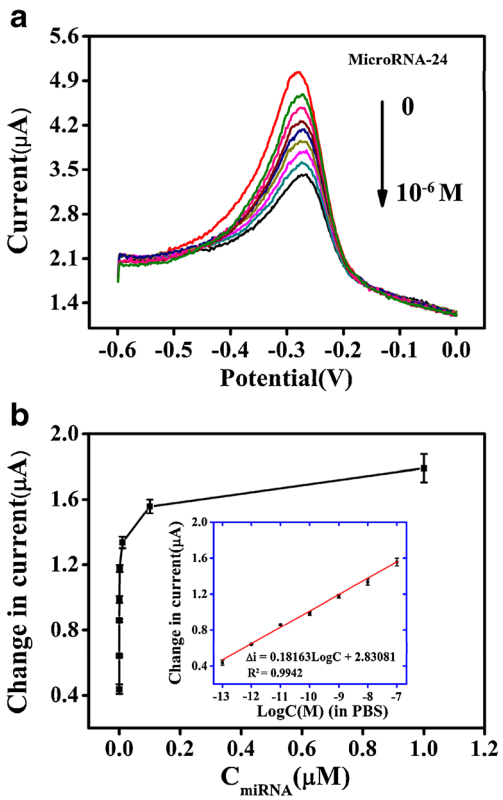

Fig. 5 **a** SWV responses of the MB-rep/probe/Au/HA/Popd/CoO/GCE toward different concentrations of target from 10^{-13} to 10^{-6} M in 0.01 M PBS (pH 7.4), **b** Changes in current of the MB-rep/probe/Au/HA/Popd/CoO/GCE as a function of target concentration. The inset shows the corresponding calibration curve. Error bars represent the standard deviations of the change in current (Δi) obtained from three repeated determinations

Table 2 Comparison of analytical performances of different methods for the detection of microRNA

Materials used	Method	Linear range	LOD	Ref.
An "off-on" fluorescent switch	Fluorescence	1 f. to 1 μM	0.75 fM	[31]
Copper nanoparticles act as a nano-dye	Fluorescence	1 pM to 1 nM	100 fM	[32]
Tetrahedral DNA nanostructure and G-wire	Electrochemistry	500 f. to 10 nM	176 fM	[13]
Nafion/CNTs/PVP/GCE	Electrochemiluminescence	40 f. to 1.0 pM	20 fM	[33]
Resonance Energy Transfer betweenAu Nanoparticles	Electrochemiluminescence	1.0 f. to 1.0 nM	0.5 fM	[34]
AuNPs@Dox@S1/Cp/MCH/Au electrode	Electrochemistry	1 pM to 10 nM	170 fM	[35]
MB-rep/Probe/Au/HA/Popd/CoO/GCE	Electrochemistry	0.1 pM to 0.1 μM	33.3 fM	This work

The displacement process was further verified with gel electrophoresis. In Fig. 3b, Lane 1, 2 and 3 corresponds to the probe, MB-reporter and the target. When MB-reporter was added to a solution containing the probe in 60 °C for 2 h, hybridization occurred and bright band was found owing to the formation of MB-rep/probe duplex (lane 4). Similar result was also observed when adding the target to the probe solution (lane 5). When the MB-rep/probe duplex was added to the target solution, a bright and a dull band were observed (lane 6). The bright band indicated the binding of target to the probe, while the dull band suggested the released MB-reporter rested in the solution and remained as a hairpin structure.

EIS evaluation of the nonspecific adsorption

Electrochemical impedance spectroscopy (EIS) was utilized to monitor the changes (charge transfer resistance, Rct) of modified electrodes with HA (MB-rep/Probe/Au/HA/Popd/CoO/GCE) and without HA (MB-rep/Probe/Au/Popd/CoO/GCE) in real human serum samples. As shown in Fig. 4, after soaking in different samples with 0%, 1%, 5%, 10%, 20%, 50% and 100% human serum (*V*/V) for 30 min in sequence, the Rct of the MB-rep/Probe/Au/Popd/CoO/GCE (Fig. 4a) increased with the concentration increase of the samples, due to the nonspecific adsorption of proteins at the electrode surface. However, for the electrode modified with HA (MB-rep/Probe/Au/HA/Popd/CoO/GCE) (Fig. 4b), no significant changes in the Rct were observed for all the studied serum concentrations, indicating excellent antifouling ability of the modified electrode.

Sensitivity and selectivity of the biosensor

The analytical performance of the biosensor was characterized using SWV method. After incubation in different concentrations of microRNA-24 for 45 min, the peak currents of the biosensor decreased accordingly with increasing concentrations of the target microRNA-24 from 0.1 pM to 0.1 μM (Fig. 5a). The calibration plot displays a good linear relationship between the peak current response and the logarithm of microRNA concentrations with a correlation coefficient of 0.9942 (Fig. 5b), and the detection limit is calculated to be 33.3 fM. The analytical performances of this method were compared with previously repoted methods, as summarized in Table 2. This result confirms that the biosensor has very wide linear range and high sensitivity for microRNA-24 determination.

The selectivity of the biosensor was investigated using high concentrations of possible interferents microR-141, microRNA-200, microRNA-429 and low concentration of the target microRNA-24. As shown in Fig. 6, the response current of microRNA-24 was significantly larger than those of microRNA-141, microRNA −200, microRNA-429, even at a much lower concentration, suggesting excellent selectivity of the biosensor towards microRNA-24.

Application of the biosensor for detection of microRNA-24 from cancer cells

The detection of microRNAs from cancer cell is of great importance to enable the biosensor for point-of-care and diagnostic tests. To investigate the practical application of the constructed biosensor, MCF-7 Cell extracts (cell lines) were used. The recoveries of various concentrations of microRNA-24 added to MCF-7 (10^6 cell) samples were detected with the biosensor, as

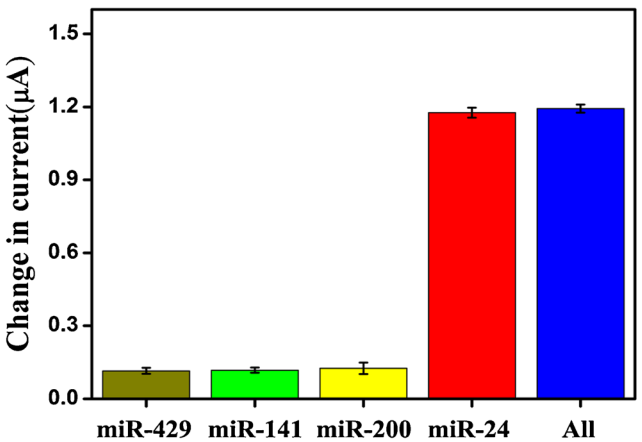

Fig. 6 Response of the biosensor to microRNA-24 (1 nM), microRNA-429 (1 μM), microRNA-141 (1 μM), microRNA-200 (1 μM), and their mixture (containing 1 nM microRNA-24, 1 μM microRNA-429, 1 μM microRNA-141, and 1 μM microRNA-200)

shown in Fig. S4. Clearly, the relative standard deviations (RSDs) are within the range from 1.3% to 3.1%, which suggests feasibility of the biosensor for real sample assays.

Conclusions

In summary, a novel antifouling biosensor based on DNA displacement method for the detection of microRNA-24 with a detection limit of 33.3 f. was developed. In the biosensor system, CoO/Popd core/shell nanopetals and AuNCs provided large effective surface area for the immobilization of a large amount of MB-rep/probe, so as to enhance the sensing signal. Taking advantage of the unique property of HA, the biosensor with HA in the sensing interface possessed excellent antifouling properties for the sensitive detection of microRNA in human serum. The successful application of this biosensor in the assay of tumor cell samples further verified its capability of practical sample analysis. It is believed that, after further simplifying the fabrication process, this antifouling biosensor with high sensitivity and excellent selectivity has great potential for application in biomedical research and early clinical diagnostics.

Acknowledgements This research was supported by the National Natural Science Foundation of China (21675093, 21422504,21505081), and the Taishan Scholar Program of Shandong Province of China (ts20110829).

Compliance with ethical standards

The author(s) declare that they have no competing interests.

References

1. Hong C, Baek A, Hah SS et al (2016) Fluorometric detection of MicroRNA using isothermal gene amplification and graphene oxide. Anal Chem 88:2999–3003. https://doi.org/10.1021/acs.analchem.6b00046
2. Li C, Li Z, Jia H, Yan J (2011) One-step ultrasensitive detection of microRNAs with loop-mediated isothermal amplification (LAMP). Chem Commun (Camb) 47:2595–2597. https://doi.org/10.1039/c0cc03957h
3. Jia H, Li Z, Liu C, Cheng Y (2010) Ultrasensitive detection of microRNAs by exponential isothermal amplification. Angew Chemie - Int Ed 49:5498–5501. https://doi.org/10.1002/anie.201001375
4. Shi C, Liu Q, Ma C, Zhong W (2014) Exponential strand-displacement amplification for detection of micrornas. Anal Chem 86:336–339. https://doi.org/10.1021/ac4038043
5. Liu H, Li L, Duan L et al (2013) High specific and ultrasensitive isothermal detection of microRNA by padlock probe-based exponential rolling circle amplification. Anal Chem 85:7941–7947. https://doi.org/10.1021/ac401715k
6. Wang XP, Yin BC, Wang P, Ye BC (2013) Highly sensitive detection of microRNAs based on isothermal exponential amplification-assisted generation of catalytic G-quadruplex DNAzyme. Biosens Bioelectron 42:131–135. https://doi.org/10.1016/j.bios.2012.10.097
7. Zhang DY, Seelig G (2011) Dynamic DNA nanotechnology using strand-displacement reactions. Nat Chem 3:103–113. https://doi.org/10.1038/nchem.957
8. Volinia S, Calin GA, Liu C-G et al (2006) A microRNA expression signature of human solid tumors defines cancer gene targets. PNAS 103:2257–2261. https://doi.org/10.1073/pnas.0510565103
9. Zhu S, Wu H, Wu F et al (2008) MicroRNA-21 targets tumor suppressor genes in invasion and metastasis. Cell Res 18:350–359. https://doi.org/10.1038/cr.2008.24
10. Ikeda S, Kong SW, Lu J et al (2007) Altered microRNA expression in human heart disease:367–373. https://doi.org/10.1152/physiolgenomics.00144.2007
11. Fiore R, Siegel G, Schratt G (2008) MicroRNA function in neuronal development, plasticity and disease. Biochim Biophys Acta - Gene Regul Mech 1779:471–478. https://doi.org/10.1016/j.bbagrm.2007.12.006
12. Taganov KD, Boldin MP, Chang K-J, Baltimore D (2006) NF-kappaB-dependent induction of microRNA miR-146, an inhibitor targeted to signaling proteins of innate immune responses. Proc Natl Acad Sci U S A 103:12481–12486. https://doi.org/10.1073/pnas.0605298103
13. Huang YL, Mo S, Gao ZF et al (2017) Amperometric biosensor for microRNA based on the use of tetrahedral DNA nanostructure probes and guanine nanowire amplification. Microchim Acta 184:2597–2604. https://doi.org/10.1007/s00604-017-2246-8
14. Wang J, Lu Z, Tang H et al (2017) Multiplexed electrochemical detection of MiRNAs from sera of glioma patients at different stages via the novel conjugates of conducting magnetic microbeads and Diblock oligonucleotide-modified gold nanoparticles. Anal Chem 89:10834–10840. https://doi.org/10.1021/acs.analchem.7b02342
15. Xu S, Gao T, Feng X et al (2016) Dual ligand co-functionalized fluorescent gold nanoclusters for the "turn on" sensing of glutathione in tumor cells. J Mater Chem B 4:1270–1275. https://doi.org/10.1039/c5tb02195b
16. Zhou Y, Li B, Wang M et al (2017) Fluorometric determination of microRNA based on strand displacement amplification and rolling circle amplification. Microchim Acta 184. https://doi.org/10.1007/s00604-017-2450-6
17. Das J, Ivanov I, Montermini L et al (2015) An electrochemical clamp assay for direct, rapid analysis of circulating nucleic acids in serum. Nat Chem 7:569–575. https://doi.org/10.1038/nchem.2270
18. Koo KM, Carrascosa LG, Shiddiky MJA, Trau M (2016) Poly(a) extensions of miRNAs for amplification-free electrochemical detection on screen-printed gold electrodes. Anal Chem 88:2000–2005. https://doi.org/10.1021/acs.analchem.5b04795
19. Jiang S, Cao Z (2010) Ultralow-fouling, functionalizable, and hydrolyzable zwitterionic materials and their derivatives for biological applications. Adv Mater 22:920–932. https://doi.org/10.1002/adma.200901407
20. Leng C, Hung HC, Sun S et al (2015) Probing the surface hydration of nonfouling Zwitterionic and PEG materials in contact with proteins. ACS Appl Mater Interfaces 7:16881–16888. https://doi.org/10.1021/acsami.5b05627
21. Yamanlar S, Sant S, Boudou T et al (2011) Surface functionalization of hyaluronic acid hydrogels by polyelectrolyte multilayer films. Biomaterials 32:5590–5599. https://doi.org/10.1016/j.biomaterials.2011.04.030
22. Huang R, Liu X, Ye H et al (2015) Conjugation of hyaluronic acid onto surfaces via the interfacial polymerization of dopamine to prevent protein adsorption. Langmuir 31:12061–12070. https://doi.org/10.1021/acs.langmuir.5b02320
23. Markham NR, Zuker M (2005) DINAMelt web server for nucleic acid melting prediction. Nucleic Acids Res 33:577–581. https://doi.org/10.1093/nar/gki591

24. Su S, Wu Y, Zhu D et al (2016) On-electrode synthesis of shape-controlled hierarchical flower-like gold nanostructures for efficient interfacial DNA assembly and sensitive electrochemical sensing of MicroRNA. Small:3794–3801. https://doi.org/10.1002/smll.201601066
25. Zhou W, Zhang J, Xue T et al (2008) Electrodeposition of ordered mesoporous cobalt hydroxide film from lyotropic liquid crystal media for electrochemical capacitors. J Mater Chem 18:905. https://doi.org/10.1039/b715070a
26. Chou S-L, Wang J-Z, Liu H-K, Dou S-X (2008) Electrochemical deposition of porous co(OH)[sub 2] Nanoflake films on stainless steel mesh for flexible supercapacitors. J Electrochem Soc 155: A926. https://doi.org/10.1149/1.2988739
27. Shang L, Dörlich RM, Brandholt S et al (2011) Facile preparation of water-soluble fluorescent gold nanoclusters for cellular imaging applications. Nano 3:2009. https://doi.org/10.1039/c0nr00947d
28. Simms GA, Padmos JD, Zhang P (2009) Structural and electronic properties of protein/thiolate-protected gold nanocluster with "staple" motif: a XAS, L-DOS, and XPS study. J Chem Phys 131. https://doi.org/10.1063/1.3268782
29. Wang W, Cui M, Song Z, Luo X (2016) An antifouling electrochemical immunosensor for carcinoembryonic antigen based on hyaluronic acid doped conducting polymer PEDOT. RSC Adv 6: 88411–88416. https://doi.org/10.1039/C6RA19169J
30. Chen C-H, Luo S-C (2015) Tuning surface charge and morphology for the efficient detection of dopamine under the interferences of uric acid, ascorbic acid, and protein adsorption. ACS Appl Mater Interfaces 7:21931–21938. https://doi.org/10.1021/acsami.5b06526
31. Li Y, Pu Q, Li J et al (2017) An "off-on" fluorescent switch assay for microRNA using nonenzymatic ligation-rolling circle amplification. Microchim Acta 184:4323–4330. https://doi.org/10.1007/s00604-017-2475-x
32. Chi BZ, Liang RP, Bin QW et al (2017) Direct fluorescence detection of microRNA based on enzymatically engineered primer extension poly-thymine (EPEPT) reaction using copper nanoparticles as nano-dye. Biosens Bioelectron 87:216–221. https://doi.org/10.1016/j.bios.2016.08.042
33. Xiong H, Zheng X (2017) Electrochemiluminescence based determination of micro-RNA using target-guided assembly of gold nanoparticles on an electrode modified with Nafion, carbon nanotubes and polyvinylpyrrolidone. Microchim Acta 184:1781–1789. https://doi.org/10.1007/s00604-017-2163-x
34. Feng Q-M, Shen Y-Z, Li M-X et al (2016) Dual-wavelength Electrochemiluminescence Ratiometry based on resonance energy transfer between au nanoparticles functionalized g-C3N4 Nanosheet and Ru(bpy)3(2+) for microRNA detection. Anal Chem 88:937–944. https://doi.org/10.1021/acs.analchem.5b03670
35. Tao Y, Yin D, Jin M et al (2017) Double-loop hairpin probe and doxorubicin-loaded gold nanoparticles for the ultrasensitive electrochemical sensing of microRNA. Biosens Bioelectron 96:99–105. https://doi.org/10.1016/j.bios.2017.04.040